Proceedings of IMECE'03
2003 ASME International Mechanical Engineering Congress
Washington, D.C., November 15–21, 2003

IMECE2003-41603

MODELING AND DISTURBANCE REJECTION CONTROL OF A NANOPOSITIONER WITH APPLICATION TO BEAM STEERING

Jason J. Gorman and Nicholas G. Dagalakis
Intelligent Systems Division
National Institute of Standards and Technology
Gaithersburg, Maryland 20899-8230
gorman@cme.nist.gov

ABSTRACT

This paper discusses the modeling and control of a nanopositioning flexure hinge mechanism with a piezoelectric actuator. A complete dynamic model for the mechanism is presented along with experimentally determined system parameters. The control design concentrates on the problem of controlling the nanopositioner when a base excitation is injected into the system. The effects of the base excitation are overcome using two approaches. The first is a robust tracking controller which is developed to cancel the excitation effect on the tracking error. The second is an inertial compensator which is designed to update the desired trajectory using base motion measurements, such that the nanopositioner performs the desired trajectory in an inertial frame. This approach is demonstrated through simulation results. These principals are being developed for use in beam steering applications which require nanoradian resolution and very low beam jitter.

INTRODUCTION

There have been significant developments in the design of nanopositioning stages in recent years. This is largely due to the many applications, both in industry and in research, which benefit from this technology. Examples of such devices include the work of Scire and Teague [1], Gao et al. [2], Chang et al. [3], and Dagalakis et al. [4]. The most common design approach for a nanopositioning stage is to create a flexure hinge mechanism which is actuated by piezoelectric actuator. There are many important criteria which must be considered in the design process, such as the travel, bandwidth and resolution of the device. Therefore, the assortment of designs presented in the literature is large and greatly varied. A general discussion on designing flexure hinge mechanisms has been discussed in detail by Smith [5].

In this paper, the modeling and control of a particular nanopositioning mechanism is discussed. The design of the nanopositioner is a single-degree-of-freedom scaled-down version of the device discussed by Dagalakis et al. [4]. One application for this device which is currently being investigated is high-precision beam steering, with an emphasis on deep space optical communications. Future interstellar explorer missions will require a high-bandwidth communications link with a terrestrial monitoring station. The most likely candidate for this link is optical communications due to its high data transfer rates and low power consumption, as discussed by Boone et al. [6]. However, one major difficulty in operating an optical communication system over such great lengths is that the beam steering mechanism must have very high positioning accuracy. As an example, when transmitting data from Jupiter, an error on the order of nanoradians can result in an error in the beam placement as large as a kilometer when the beam reaches Earth. Although there have been many beam steering mechanisms used in aerospace applications, none of the commercially available devices have tracking accuracy and resolution on the order of a nanoradian. Therefore, new devices and their associated control systems must be developed to enable future space missions.

A nanopositioning mechanism could provide the level of precision motion control required by a deep space optical communication system. However, most nanopositioning applications have much lower dynamic performance requirements as compared to beam steering. Furthermore, the operational conditions for nanopositioners used in typical applications, such as microscopy, are very different compared to operation in a spacecraft. Therefore, the research presented in this paper concentrates on developing an accurate model and high performance controller for a nanopositioner, which will enable future beam steering applications.

Steering a laser beam from a spacecraft presents several difficulties. Most importantly, the motion of the spacecraft results in a disturbance to the beam steering mechanism causing beam jitter. This can be viewed as the standard base excitation problem studied in vibration control. The base excitation causes beam steering errors in two distinct ways. The first is by

inducing vibrations in the beam steering mechanism. The second is by causing displacements of the beam steering mechanism with respect to an inertial reference frame. The end result is an error in the angle of the steered beam along with an offset in the point of departure of the beam. In most cases, the angle error will be of much greater significance than the beam offset.

As an initial step towards using a nanopositioner for beam steering applications, a dynamic model including the base excitation and a controller designed to compensate for the excitation will be presented. The model combines the characteristics of the flexure hinge mechanism and piezoelectric actuator, along with the coupling to the excitation. Using this model, a robust tracking controller has been developed which compensates for the disturbance. The controller utilizes an estimate of the disturbance and a sliding mode controller to guarantee a bounded tracking error. Furthermore, an inertial compensator is used to provide a desired trajectory to the controller which will maintain the required pointing trajectory when the spacecraft is moving in an inertial frame.

First, a discussion on using a nanopositioner for beam steering will be presented. Then the dynamic model will be derived and the results of model verification experiments are discussed. This will be followed by the development of the robust tracking controller and inertial compensator. Simulations results for the control approach are then presented and discussed. Finally, conclusions on the presented work are provided.

NANOPOSITIONER DESIGN AND BEAM STEERING

A single degree of freedom nanopositioner is shown in Fig. 1. The nanopositioner design is comprised of a flexure hinge mechanism, a piezoelectric actuator, and a spherical flexure hinge coupler between the actuator and the flexure hinge mechanism. This design is based on the mechanism previously discussed by Dagalakis et al. [4], but the scale of the mechanism has been reduced by a factor of four. This particular design has been shown to have very low cross-talk errors between motion axes. In addition, angular deviations have also been determined to be very small compared to other mechanisms. Further details on the performance of this mechanism design can be found in [4].

The reduction in scale is motivated by an interest in utilizing the design concept presented in [4] to make meso and, eventually, micro devices. The area of the flexure hinge mechanism and piezoelectric actuator for the current device is 46 mm x 46 mm. The flexure hinge mechanism has ten right circular flexure hinges, as indicated by the numbering in Fig. 1b. A parallel lever design is used to amplify the motion of the piezoelectric actuator. The amplification gain ratio is determined by the geometry of the four levers. The length of the input end of the lever, which is the section between flexures 1 and 3, is denoted as a, and the length of the output end of the lever, which is the section between flexures 3 and 5, is denoted as b. Therefore, the amplification gain ratio is b/a. This ratio has been set to ten in the existing mechanism. Based on this amplification, the nanopositioner has a range of 0 μm to 91 μm for an input voltage range of the 0 V to 150 V for the piezoelectric actuator.

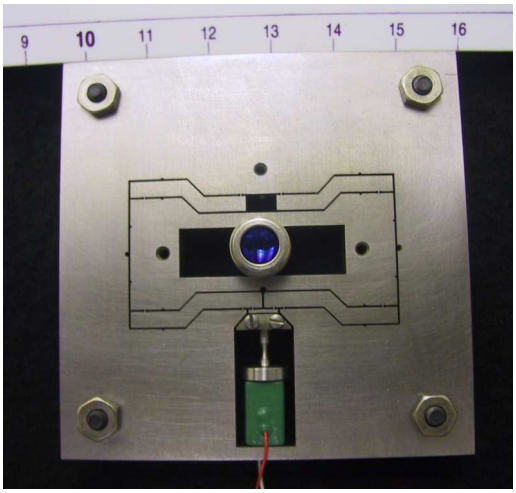

(a)

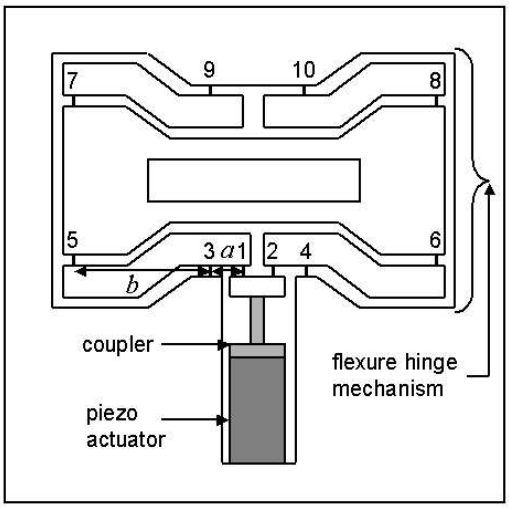

(b)

Fig. 1 Single degree of freedom nanopositioner a) photograph b) schematic

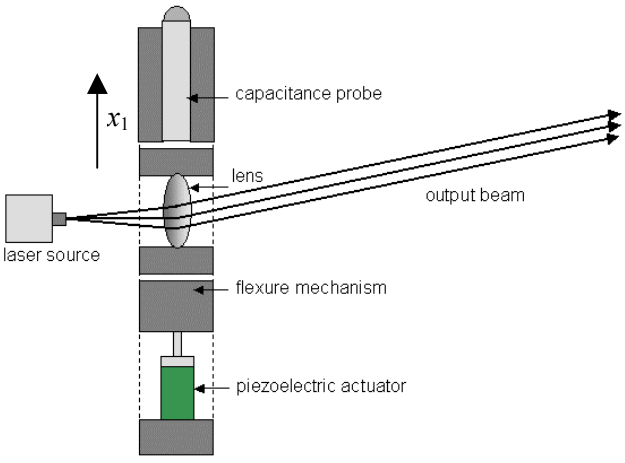

Fig. 2 Beam steering using a nanopositioner, lens, and a stationary laser source

This design can be used as a beam steering mechanism using the simple approach depicted in Fig. 2. An aspheric lens is attached to the nanopositioner, which is positioned one focal length, f, from an optical fiber emitting a laser beam, resulting in a collimated output beam. By moving the nanopositioner perpendicular to the beam, by a displacement x_1, the output beam angle, φ, is related to the nanopositioner translation such that $\varphi = x_1 / f$, based on the small angle approximation. When the focal length is in the range of a few millimeters, the expected beam steering angle range is on the order of milliradians. The beam angle depicted in Fig. 2 is only drawn to demonstrate the concept and does not represent the actual beam angle range of the mechanism. A capacitance probe is built into the nanopositioner to measure the displacement of the stage which can then be related to the beam angle. The range and resolution of the beam steering can be optimized by the proper selection of the lens, the position sensor, and the travel limits of the nanopositioner. The modeling of this device, including the base excitation effects which can limit the steering accuracy, will be discussed in the following section.

DYNAMIC MODELING

An accurate dynamic model of the nanopositioner shown in Fig. 1 is required to develop a model-based control design. The model will be derived in this section by considering the flexure hinge mechanism and piezoelectric actuator separately. Then the two models will be combined. The flexure hinge mechanism model will include the inertial forces resulting from a base excitation. The derived model will then be used to develop a robust tracking controller in the next section.

A breakdown of the two subsystems, flexure hinge mechanism and piezoelectric actuator, is shown in Fig. 3. In Fig. 3a, the flexure hinge mechanism is depicted including the base excitation, x_e. The position of the main (or output) stage with respect to a local reference frame is defined as x_1, the rotation angle for each of the four lever arms is defined as θ, and the position of the input stage with respect to a local reference frame is defined as x_2. The mass of the main stage, the input stage and a single lever arm are m_1, m_2, and m_3, respectively. This mechanism is kinematically over constrained and it can only move due to the rotational and translational compliance of the flexure hinges. However, the translational deflection of the hinges is expected to be much smaller than the rotational deflection.

The first step in determining the dynamic model is to find a relationship between the motion of the input stage, the output stage and the lever arms. The relationship between x_1, x_2 and θ can be determined to be:

$$\sin\theta = \frac{x_1}{b} = \frac{x_2}{a} \tag{1}$$

Therefore,:

$$x_2 = \frac{a}{b}x_1 \qquad \theta \approx \frac{1}{b}x_1 \tag{2), (3}$$

These relations will be used to place the equation of motion in terms of only x_1.

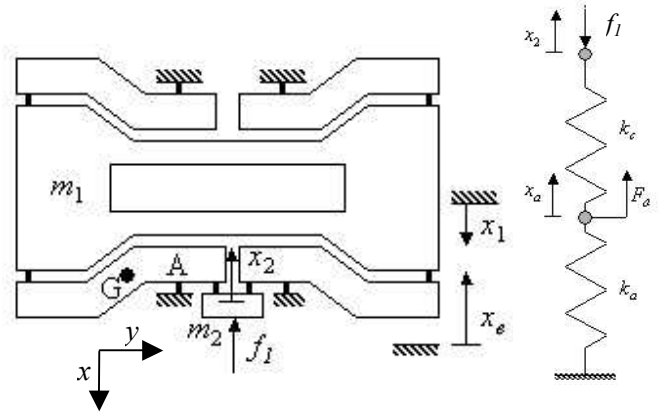

(a) (b)

Fig. 3 Schematic of (a) flexure hinge mechanism and (b) piezoelectric actuator and actuator coupler

The Lagrangian approach is used to determine the equation of motion for the nanopositioner. Therefore, the kinetic and potential energy for the system is first examined. The kinetic energy of the flexure hinge mechanism includes contributions from the inertia of the main stage, m_1, the input stage, m_2, and the lever arms, which have a mass, m_3, and mass moment of inertia, I_A, about the pivot point, A. Due to the base excitation, the linear and rotational velocities of each of the linkages must be determined in the inertial frame. Furthermore, the resulting motion of the lever arms is a general planar motion. Therefore, the kinetic energy of the flexure hinge mechanism can be written as:

$$T = \frac{1}{2}m_1(\dot{x}_1 - \dot{x}_e)^2 + \frac{1}{2}m_2(\dot{x}_2 + \dot{x}_e)^2 + \frac{1}{2}4I_G\dot{\theta}^2 + \frac{1}{2}4m_3(\dot{x}_G^2 + \dot{y}_G^2) \tag{4}$$

where $\dot{x}_G$ and $\dot{y}_G$ are Cartesian velocities of the center of mass for the lever arms, and I_G is the mass moment of inertia about the center of mass. The velocities, $\dot{x}_G$ and $\dot{y}_G$, can be found to be:

$$\dot{x}_G = -d\dot{\theta}\cos\theta + \dot{x}_e \tag{5}$$

$$\dot{y}_G = -d\dot{\theta}\sin\theta \tag{6}$$

The parameter, d, is the distance between the pivot point, A, and the center of mass, G (see Fig. 3).

The potential energy for the flexure hinge mechanism results from the stiffness of the stage. This stiffness can be difficult to model using a simple analytical expression. Discrete spring models have been derived by Paros and Weisbord [7] and discussed extensively by Smith [5]. However, due to the over constrained design, the stiffness is more complex than a simple torsional spring model. Instead of modeling the springs directly, an experimental approach was taken. Experimental results, which will be discussed shortly, indicate that the stiffness is linear for the displacement range of interest. Therefore, the stiffness of the mechanism can be

lumped into a single constant parameter, k_m, such that the potential energy can be written as:

$$V = \frac{1}{2} k_m x_1^2 \tag{7}$$

where k_m will be determined experimentally.

The equation of motion can be determined by applying Lagrange's equation, which is:

$$\frac{d}{dt}\left(\frac{\partial L}{\partial \dot{x}_1}\right) - \frac{\partial L}{\partial x_1} = Q \tag{8}$$

and the Lagrangian, L, is defined as $L = T - V$. The generalized force, Q, is chosen as:

$$Q = -B\dot{x}_1 + \frac{a}{b} f_1 \tag{9}$$

where the first term accounts for structural damping, where B is the damping parameter, and the second is the input force, f_1, from the actuator and coupler. Therefore, by applying Eq. (8) based on Eqs. (2)-(7) and (9), the following equation of motion results:

$$M\ddot{x}_1 + B\dot{x}_1 + k_m x_1 = \frac{a}{b} f_1 + M_e \ddot{x}_e \tag{10}$$

where:

$$M = m_1 + \frac{a^2}{b^2} m_2 + 4\frac{I_A}{b^2} \tag{11}$$

$$M_e = m_1 - \frac{a}{b} m_2 + 4\frac{d}{b} m_3 \tag{12}$$

The second term on the right hand side of Eq. (10) represents the inertial force due to the excitation.

Next, an electromechanical model of the piezoelectric actuator and actuator coupler is derived. Due to the small mass of the actuator and coupler compared to the flexure hinge mechanism, it is assumed that they act as massless spring elements. A schematic of their configuration is shown in Fig. 3b. The objective in modeling the actuator and coupler is to find a relationship between the force applied to the flexure hinge mechanism, f_1, the displacement x_1, and the actuator force, F_a. By summing the forces at the two spring junctions, the following equations result:

$$f_1 + k_c(x_2 - x_a) = 0 \tag{13}$$

$$F_a - k_a x_a + k_c(x_2 - x_a) = 0 \tag{14}$$

where k_c is the stiffness coefficient for the actuator coupler and k_a is the stiffness coefficient for the piezoelectric actuator. These parameters can be determined either analytically or experimentally. In this case, the actuator stiffness is calculated based on the manufacturer's specifications and the coupler stiffness is found using a relation for a spherical hinge discussed in [5]. Solving Eqs. (13) and (14) simultaneously and using Eq. (2) gives an expression for the applied force, f_1, such that:

$$f_1 = -\frac{a}{b}\frac{k_a k_c}{k_a + k_c} x_1 + \frac{k_c}{k_a + k_c} F_a \tag{15}$$

An expression for the actuator force, F_a, must also be determined. Based on the model presented by Goldfarb and Celanovic [8], the electrical dynamics of a piezoelectric actuator can be written as:

$$q = T x_1 + C v_t \tag{16}$$

$$v_t = v_{in} - v_{rc} \tag{17}$$

$$F_a = T v_t \tag{18}$$

where q is the charge of the actuator, T is the actuator transformer ratio, C is the actuator capacitance, v_{in} is the voltage applied to the actuator, and v_{rc} is an internal voltage. It is well known that piezoelectric actuators have a hysteresis nonlinearity between the applied voltage and resulting charge of the actuator. This results in errors in displacement when voltage is used as the control input. Goldfarb and Celanovic [8] describe the hysteresis effect caused by v_{rc} in detail and provide an effective approach to estimating the hysteresis. In this paper, this internal voltage will be viewed as an unknown disturbance, so a complete model of the nonlinearity is not required. However, Goldfarb and Celanovic's approach could be used to estimate the internal voltage and then use the estimate as a feedforward component of the controller.

The final equation of motion can be found by combining Eqs. (10), (15), (17), and (18), resulting in the following:

$$M\ddot{x}_1 + B\dot{x}_1 + Kx_1 = \frac{a}{b}\frac{k_c T}{k_a + k_c} v_{in} + \delta \tag{19}$$

where:

$$K = k_m + \frac{a^2}{b^2}\frac{k_a k_c}{k_a + k_c} \tag{20}$$

$$\delta = M_e \ddot{x}_e - \frac{a}{b}\frac{k_c T}{k_a + k_c} v_{rc} \tag{21}$$

The dynamic model, shown in Eq. (19), is a linear second order system with a nonlinear disturbance, δ. Therefore, the only difficulty in controlling this system comes from the disturbance, which is a combination of the internal voltage of the actuator which causes hysteresis, and inertial forces resulting from the base excitation. An approach for compensating for these disturbance forces will be discussed shortly. First, the experimentally determined system parameters will be presented.

SYSTEM PARAMETERS AND OPEN LOOP TESTS

Most of the parameters in the equation of motion shown in Eq. (19) can easily be calculated or measured, such as the mass and dimensions. However, the stiffness of the flexure

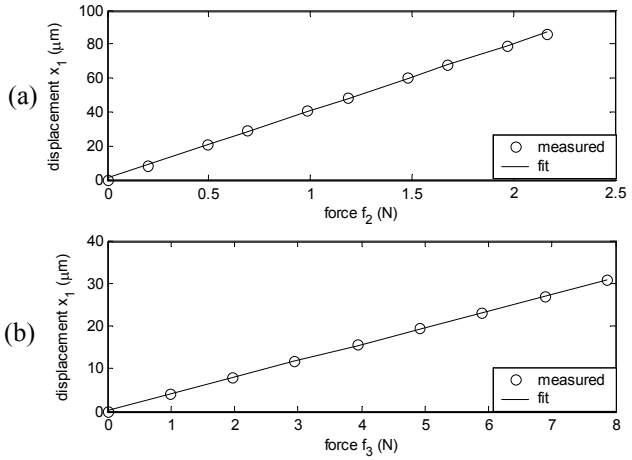

Fig. 4 Flexure mechanism static stiffness evaluation tests

mechanism, k_m, and the transformer ratio of the actuator, T, must be determined experimentally. The static force-displacement relationship for the flexure mechanism when a force is applied directly to the main stage is:

$$k_m x_1 = f_2 \tag{22}$$

A static loading stiffness test was performed on the mechanism to determine the experimental value of k_m. This was executed by applying calibrated loads to the nanopositioner while measuring the displacement. The results of this test are shown in Fig. 4a. It is clear that the stiffness of the mechanism is linear within the working region, as assumed in the modeling. As an additional verification of the parameters, a second test was performed in which the force was applied at the actuator input. This scenario can be represented by the following equation:

$$k_m x_1 = \frac{a}{b} f_3 \tag{23}$$

Comparing Eqs. (22) and (23) indicates that the second test can be used to verify the motion amplification of the mechanism. The results of this test are shown in Fig. 4b. A comparison of the results of two tests confirms the motion amplification ratio, b/a, to be approximately equal to ten since this is the factor between the slopes of each of the plots.

A final static test was performed on the fully assembled nanopositioner to determine the transformer ratio, T. The static relation between the applied voltage, v_{in}, and displacement, x_1, was determined experimentally as shown in Fig. 5. This plot shows the expected hysteresis loop for an increasing and then decreasing voltage. These results can be compared to the equation resulting from applying static analysis to the equation of motion in Eq. (19). This results in the following equation:

$$\left(k_m + \frac{a^2}{b^2} \frac{k_a k_c}{k_a + k_c} \right) x_1 = \frac{a}{b} \frac{k_c T}{k_a + k_c} v_{in} \tag{24}$$

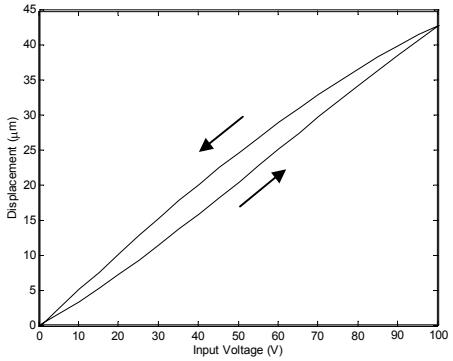

Fig. 5 Static open-loop force-displacement relationship

Table 1 Nanopositioner Model Parameters

	value		value
k_m	25149 N/m	I_a	2.145×10^{-7} kg m^2
k_a	1.859×10^8 N/m	C	0.73 μF
k_c	2.440×10^7 N/m	T	9.06 C/m
m_1	0.0193 kg	a	1.46×10^{-3} m
m_2	0.0013 kg	b	1.49×10^{-2} m
m_3	0.0025 kg	d	8.1×10^{-3} m

All of the parameters in Eq, (24) are known at this point except for T. Therefore, by finding the slope of the nearly linear rising curve in the data shown in Fig. 5, and utilizing Eq. (24), the transformer ratio, T, can be estimated. A more accurate approach for determining the transformer ratio would require measuring the charge on the actuator, which was not considered in this initial research. The complete set of parameter values are listed in Table 1. These values have been used in the simulation tests which will be discussed later. First, an approach to controlling the nanopositioner based on the derived model will be discussed.

DISTURBANCE REJECTION CONTROL

In many typical nanopositioning applications, such as microscopy and mask alignment, the operating environment is well controlled and the required tracking bandwidth is low. Therefore, the specifications for the control design can generally be achieved using standard linear approaches, even with the presence of actuator hysteresis. However, the use of nanopositioners for beam steering in an optical communication system presents several difficulties typically not addressed in the control of nanopositioning mechanisms.

High bandwidth beam steering can be severely affected by actuator hysteresis, since it introduces a phase lag, causing large tracking errors and possible instability. Furthermore, the base excitation, which can be expected in many beam steering applications, results in inertial disturbances to the mechanism as well as line-of-sight perturbations. Both of which can result in tracking errors. In this section, a robust control approach is presented which is designed to compensate for the base excitation and hysteresis.

The control system concept proposed for the nanopositioning mechanism is shown in Fig. 6. This system is

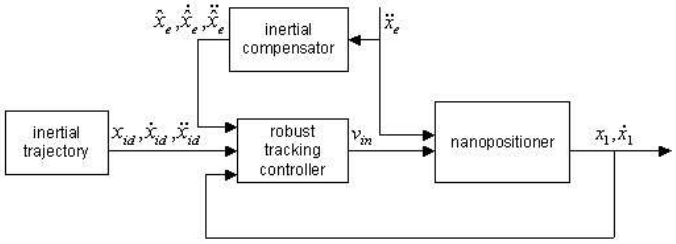

Fig. 6 Block diagram of control system for beam steering

decomposed into two sub-systems, the robust tracking controller and the inertial compensator. The robust tracking controller is used to overcome the hysteresis and base excitation disturbance to achieve high precision motion control. This is achieved with a sliding mode controller and feedback from an accelerometer measuring the base excitation. The inertial compensator adjusts the desired trajectory based on estimates of the base motion, which are found by integrating the accelerometer signal.

Robust Tracking Control

The goal of the robust tracking control design is to achieve a guaranteed bounded tracking error for a given level of base excitation and hysteresis effect. There are a number of approaches which could be adopted for this purpose. The internal model principle is one which is well suited for base excitation problems when the frequency of the excitation is known or can be estimated online. Alleyne and Pomykalski [9] have investigated the use of an internal model for nonlinear systems such as the system discussed in this paper. Linear robust control could also be used to minimize the effect of the hysteresis and external disturbances, which has been examined by Salapaka et al. [10]. However, due to the boundedness of the uncertainty in the base excitation and hysteresis, sliding mode control has been chosen. This will provide broadband disturbance rejection and it is straightforward to design the controller for the presented system. Shan and Menq [11] have demonstrated the use of sliding mode control for disturbance rejection in a micropositioning magnetic suspension stage. A similar approach is utilized here, with adaptations to include the base excitation measurement data and base motion estimates. First, the system dynamics are transformed into error coordinates using the relations $\tilde{x}_1 = x_1 - x_{1d}$ and $\tilde{x}_2 = \dot{x}_1 - \dot{x}_{1d}$, such that:

$$\dot{\tilde{x}}_1 = \tilde{x}_2 \tag{25}$$

$$\dot{\tilde{x}}_2 = -\frac{K}{M}x_1 - \frac{B}{M}x_2 - \ddot{x}_{1d} + \frac{\delta}{M} + \frac{a}{b}\frac{k_c T}{M\left(k_a + k_c\right)}v_{in} \tag{26}$$

Since the system, represented in Eqs. (25-26), has linear second order dynamics with a nonlinear disturbance, the design of the sliding mode controller is straightforward. This approach has been discussed in detail by Edwards and Spurgeon [12], among others. Therefore, only an outline of the approach is provided here. A first order sliding surface, s, is chosen such that:

$$s = \tilde{x}_2 + \lambda \tilde{x}_1 \tag{27}$$

where λ is a positive valued design parameter. The sliding surface is designed such that when the system states lie on this surface, the system is exponentially stable. Therefore, the problem is reduced to guaranteeing that the system reaches the sliding surface, or in the case of bounded tracking, some region around the surface. The sliding surface dynamics are determined by taking the time derivative of Eq. (27), and applying Eq. (25-26). This results in the following:

$$\dot{s} = -\frac{K}{M}x_1 - \frac{B}{M}x_2 - \ddot{x}_{1d} + \frac{\delta}{M} + \lambda\tilde{x}_2 + \frac{a}{b}\frac{k_c T}{M\left(k_a + k_c\right)}v_{in} \tag{28}$$

Based on the sliding dynamics, the control law for the applied voltage, v_{in}, is chosen as:

$$v_{in} = -\frac{b}{a}\frac{M\left(k_a + k_c\right)}{k_c T}\left(-\frac{K}{M}x_1 - \frac{B}{M}x_2 - \ddot{x}_{1d} + \frac{\hat{\delta}}{M} + \lambda\tilde{x}_2 + \phi s + \frac{\rho s}{\left(s^2 + \varepsilon^2\right)^{1/2}}\right) \tag{29}$$

where:

$$\hat{\delta} = M_e \ddot{\hat{x}}_e \tag{30}$$

The parameter ϕ is a positive valued design constant, and the variables $\ddot{\hat{x}}_e$ is an estimate of the actual disturbance variable, $\ddot{x}_e$. This estimate will be determined by the inertial compensator, which will be discussed shortly. The switching gain, ρ, is a positive definite function which will be chosen to guarantee a desired tracking error bounds. The final term in Eq. (29) is a continuous approximation to the standard discontinuous sliding mode control switching law. Substituting Eq. (29) into Eq. (28) results in the following closed-loop sliding surface dynamics:

$$\dot{s} = -\phi s - \frac{\rho s}{\left(s^2 + \varepsilon^2\right)^{1/2}} + \frac{\delta - \hat{\delta}}{M} \tag{31}$$

It is clear from Eq. (31) that if the difference between the actual and estimated disturbances were equal to zero, then the system would be asymptotically stable. The error between the actual and estimated values can be compensated by the choice of the switching gain, ρ. This error can be written as:

$$\delta - \hat{\delta} = -\frac{a}{b}\frac{k_c T}{k_a + k_c}v_{rc} + M_e\left(\ddot{x}_e - \ddot{\hat{x}}_e\right) \tag{32}$$

In order to achieve the boundedness properties of sliding mode control, the switching gain is chosen such that $\rho > \left|\delta - \hat{\delta}\right| / M$.

Therefore it is found that:

$$\rho = \frac{\eta}{M}\left(\frac{a}{b}\frac{k_c T}{k_a + k_c} v_{rc}^* + M_e \varphi_1\right) \tag{33}$$

where $\eta > 1$, $|v_{rc}| \le v_{rc}^*$, and $\left|\ddot{x}_e - \ddot{\hat{x}}_e\right| \le \varphi_1$. Sufficient values for v_{rc}^* and φ_1 can be determined experimentally and from *a priori* bounds on the excitation, if available. It is important to note that the closed loop system is bounded-input bounded-output stable. Therefore, even if these bounds are not met, the response is guaranteed to be bounded. This property is very useful since it allows for the experimental tuning of the switching gain without risk of instability. However, when the parameters are chosen to meet these bounds, the tracking error is guaranteed to asymptotically approach a bound such that:

$$|x_1| \le \eta \Big/ \left(\lambda\left(\eta^2 - 1\right)^{1/2}\right) \tag{34}$$

The controller presented in this section in based on available estimates of the base excitation. The approach for finding these estimates and applying them to inertial compensation is discussed in the following section.

Inertial Compensator

The presented robust tracking controller can achieve a bounded tracking error for a desired trajectory within its local reference frame when an accurate estimate for $\ddot{x}_e$ is available. Furthermore, the base motion estimates can be used to update the desired trajectory so that the correct trajectory is executed in the inertial reference frame. The position of the nanopositioning stage in an inertial frame, x_i, can be written as:

$$x_i = x_1 - x_e \tag{35}$$

Therefore, assuming that the base motion, x_e, can be estimated by $\hat{x}_e$, the desired position trajectory can be written as:

$$x_{1d} = x_{id} + \hat{x}_e \tag{36}$$

where x_{id} is the desired position trajectory in the inertial frame. The desired velocity and acceleration trajectories can be found by taking the first and second derivatives of Eq. (36).

Therefore, both the robust tracking controller and the desired trajectory will require the estimated variables. The most obvious approach for obtaining these estimates is to measure the acceleration of the base of the nanopositioner using an accelerometer, and then integrate this signal for velocity and position. This approach is common in many inertial navigation systems. It has also been demonstrated for a beam steering application by Borello et al. [13].

The proposed estimation scheme is shown in Fig. 7. The measured acceleration is first passed through a low pass filter with a cut-off frequency corresponding to the nanopositioner bandwidth. The output of the low-pass filter then goes through a high-pass filter designed to cut off any DC acceleration. The

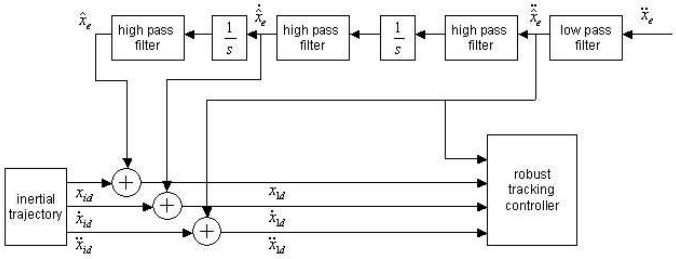

Fig. 7 Integration and filtering scheme for base excitation estimation

output of this filter is the estimate $\ddot{\hat{x}}_e$. Passing this estimate through an integrator and a second similar high-pass filter results in the estimate $\dot{\hat{x}}_e$. The second high-pass filter is used to cancel any DC content resulting from ambiguity in the initial condition for integration. Finally, $\dot{\hat{x}}_e$ is passed through an integrator and the third high-pass filter, resulting in $\hat{x}_e$.

Due to the use of the filters, the estimates will not correspond exactly to the actual variables. However, this is in some respects beneficial. Since the nanopositioner cannot track a constant acceleration due to travel limitations, it wouldn't be sensible to feed the actual signal into the controller. This particular integration and filtering scheme will capture all of the periodic content in the acceleration signal within the nanopositioner bandwidth, which is what is of the most interest when trying to stabilize the line-of-sight in a beam steering application. Of course, errors in the estimates will also exist due to the added phase lag and amplitude attenuation of the filters. Therefore, the performance limitations of the beam steering mechanism will be a factor of the controller bandwidth and the estimation bandwidth.

The robust tracking controller will receive a total of four variables based on this estimation scheme. They are $\ddot{\hat{x}}_e$, which is used to cancel the forces due to the base excitation, and $\dddot{\hat{x}}_{1d}$, $\ddot{\hat{x}}_{1d}$, and $\dot{\hat{x}}_{1d}$, which provide a full state trajectory to compensate for the motion in the inertial frame caused by the base excitation. The implementation results of the robust tracking controller and inertial compensator will be discussed in the following section.

SIMULATION RESULTS

The two-part controller discussed in the previous section was tested in simulation on the presented dynamic model. The closed-loop system, using the robust tracking controller, was designed to have the same natural frequency as the open loop system, which is ω_n = 3166.8 rad/s, and a damping ratio, ξ = 1.1. The desired trajectory in the inertial frame was a 10 Hz sinusoidal trajectory with an amplitude of 5 μm and an offset of 20 μm. Another sinusoidal signal was used as the base excitation, which had an amplitude of 10 μm and a 40 Hz frequency. As an initial test, the switching gain, ρ, and the base excitation estimates were set to zero, resulting in a PD

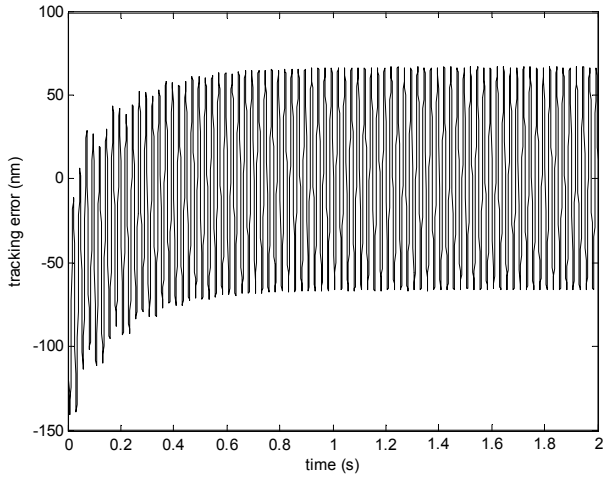

Fig. 8 Tracking error using PD Controller

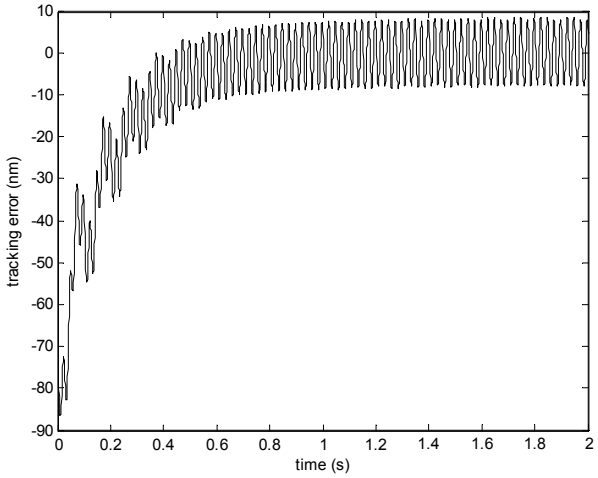

Fig. 9 Tracking error using PD controller and excitation estimates

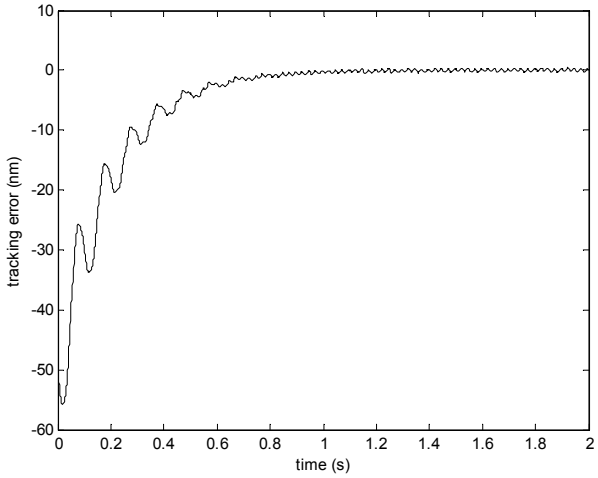

Fig. 10 Tracking error using robust tracking controller

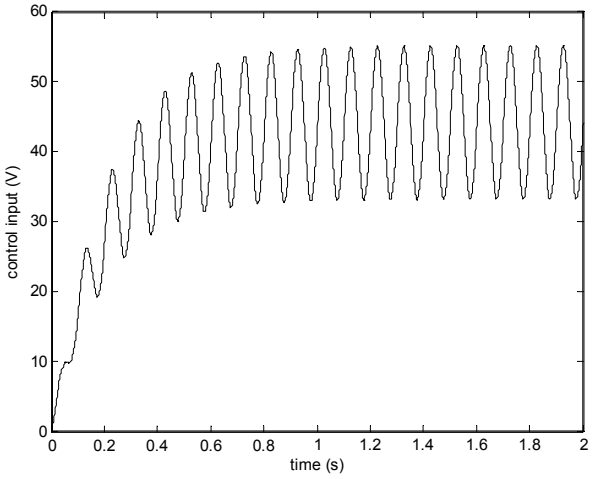

Fig. 11 Control effort when using robust tracking controller

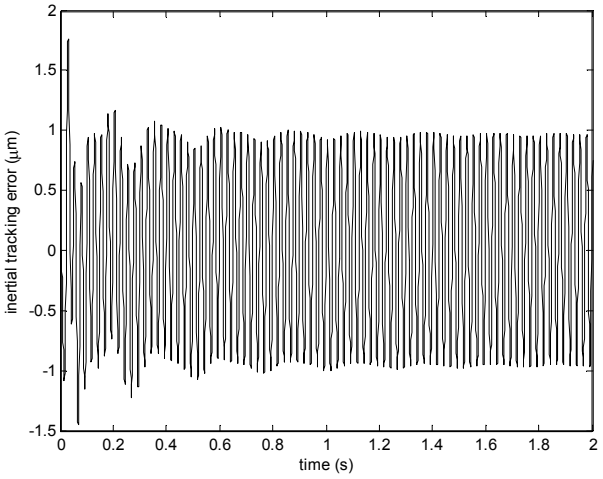

Fig. 12 Inertial tracking error

controller. The local tracking error results of this test are shown in Fig. 8, where the steady state error is on the order of ± 65 nm.

In a second test, the base excitation estimates were used in the controller but the switching gain, ρ, was still set to zero. The local tracking error results for this test are shown in Fig. 9. The use of the base excitation estimates results in a large improvement in the error, although it is still on the order of ± 10 nm. Finally, the full robust tracking controller was implemented, resulting in the local tracking error as shown in Fig. 10. In this case, the local tracking error has been reduced to ± 0.4 nm. This error is on the order of what would be acceptable for a deep space optical communication system. Furthermore, the control effort for this level of tracking performance is very reasonable, as shown in Fig. 11. The magnitude of the input voltage is similar to that resulting from a feedforward controller. Furthermore, the input is sufficiently smooth indicating that chattering does not occur. This is due to the use of the continuous sliding mode switching function.

All of these tracking error bounds are for the position of the nanopositioner in its local reference frame. The inertial compensator provides an updated trajectory for the robust tracking controller based on the base excitation estimates. Therefore, the inertial tracking error can only be as good as the excitation estimates. This can be seen in the results for the inertial tracking error as shown in Fig. 12. In the inertial frame, the tracking error is on the order of ± 1 μm. This indicates that the motion due to the base excitation has been attenuated by 90 %. Whether this reduction is acceptable is dependent on the design of the optical communication system. For example, if the base excitation effects the laser source and nanopositioner equally, then the error will result in a position bias of the beam on the order of a few micrometers. This would not have any effect on the operation of the optical communication system. However, if the base excitation causes motion in the nanopositioner and not in the laser source, then the errors would cause large errors in the beam angle.

These simulation results indicate that the robust tracking controller can effectively compensate for the inertial forces resulting from the base excitation and provide an acceptable tracking error for the nanopositioner in its local frame. However, within the inertial frame, the tracking error is significantly larger. This problem lies within the excitation estimation scheme. Due to the high-pass filtering and integration, there is phase lag and amplitude attenuation in the estimates. If better performance with respect to inertial tracking is required, a more advanced estimation scheme can be designed to reduce the tracking error.

CONCLUSION

The application of a nanopositioning mechanism to beam steering applications has been proposed due to their high-precision positioning capabilities. However, most research on the control of nanopositioners has not addressed the problems encountered in beam steering applications such as the inertial forces and beam jitter introduced by base excitations. In this paper, a model of a single degree-of-freedom nanopositioner, including the effects of a base excitation, has been presented. Using this model, a disturbance rejection controller comprised of two parts, the robust tracking controller and the inertial compensator, has been developed. The robust tracking controller combines a sliding mode controller with base excitation estimates to guarantee a desired tracking error performance within the local reference frame of the nanopositioner. The inertial compensator provides the estimates of the base excitation for the robust tracking controller and generates an update to the desired trajectory based on the base motion. This update is designed to cancel the relative motion so that beam jitter could be eliminated.

Simulation results for this control approach have been presented which show that the local tracking error is less than a nanometer but the inertial tracking error is on the order of a micrometer. This is caused by the inertial compensator which suffers from phase lag and amplitude attenuation due to the required filtering. A test bed for beam steering is currently being developed to study the relevant control problems such as base excitations and uncertainties within the optical geometry. In addition, the effect of actuator hysteresis on the tracking performance will be examined.

ACKNOWLEDGEMENTS

This research was performed while the first author held a National Research Council Postdoctoral Research Associateship Award at the National Institute of Standards and Technology.

REFERENCES

[1] Scire, F. E. & Teague, E. C., 1978, "Piezodriven 50-μm range stage with subnanometer resolution", *Review of Scientific Instruments*, **49**, pp. 1735-1740.

[2] Gao, P., Swei, S.-M., & Yuan, Z., 1999, "A new piezodriven precision nanopositioning stage utilizing flexure hinges", *Nanotechnology*, **10**, pp. 394-398.

[3] Chang, S. H., Tseng, C. K., & Chien, H. C., 1999, "An ultra-precision XYθ_Z piezo-nanopositioner part I: design and analysis", *IEEE Transactions on Ultrasonics, Ferroelectrics, and Frequency Control*, **46**, pp. 897-905.

[4] Dagalakis, N. G., Kramar, J. A., Amatucci, E., & Bunch, R., 2001, "Kinematic modeling and analysis of a planar micro-positioner", *Proceedings of the ASPE Annual Meeting*, Crystal City, VA, pp. 135-138.

[5] Smith, S. T., 2000, *Flexures: Elements of Elastic Mechanisms*, Gordon & Breach, Amsterdam.

[6] Boone, B. G., Bokulic, R. S., Andrews, G. B., McNutt, R. L. Jr., & Dagalakis, N., 2002, "Optical and microwave communications system conceptual design for a realistic interstellar explorer", *Proceedings of the SPIE - Free-Space Laser Communication and Laser Imaging II*, SPIE Vol. 4821, Seattle, WA, pp. 225-236.

[7] Paros, J. M. & Weisbord, L., 1965, "How to design flexure hinges", *Machine Design*, **37**, pp. 151-156.

[8] Goldfarb, M. & Celanovic, N., 1997, "Modeling piezoelectric stack actuators for control of micromanipulation", *IEEE Control Systems Magazine*, **17**, pp. 69-79.

[9] Alleyne, A. & Pomykalski, M., 2000, "Control of a class of nonlinear systems subject to periodic exogenous signals", *IEEE Transactions on Control Systems Technology*, **8**, pp. 279-287.

[10] Salapaka, S., Sebastian, A., Cleveland, J. P., & Salapaka, M. V., 2002, "High bandwidth nano-positioner: a robust control approach", *Review of Scientific Instruments*, **73**, pp. 3232-3241.

[11] Shan, X. & Menq, C.-H., 2002, "Robust disturbance rejection for improved dynamic stiffness of a magnetic suspension stage", *IEEE/ASME Transactions on Mechatronics*, **7**, pp. 289-295.

[12] Edwards, C. & Spurgeon, S. K., 1998, *Sliding Mode Control: Theory and Applications*, Taylor & Francis, London.

[13] Borrello, M. A., Leslie, D., & Hyman, H., 2002, "Shipboard disturbance control for the rapid optical beam steering (ROBS) pointing and tracking system", *Proceedings of the American Control Conference*, Anchorage, AK, pp. 3186-3190.